UCRL-JC-121597
PREPRINT
CONF-950793--34

Hyperspectral Imaging in the Infrared using LIFTIRS

Charles L. Bennett, Michael R. Carter, David J. Fields

International Symposium on Optical Science, Engineering and Instrumentation,
July 9-14, 1995, San Diego, California

July, 1995

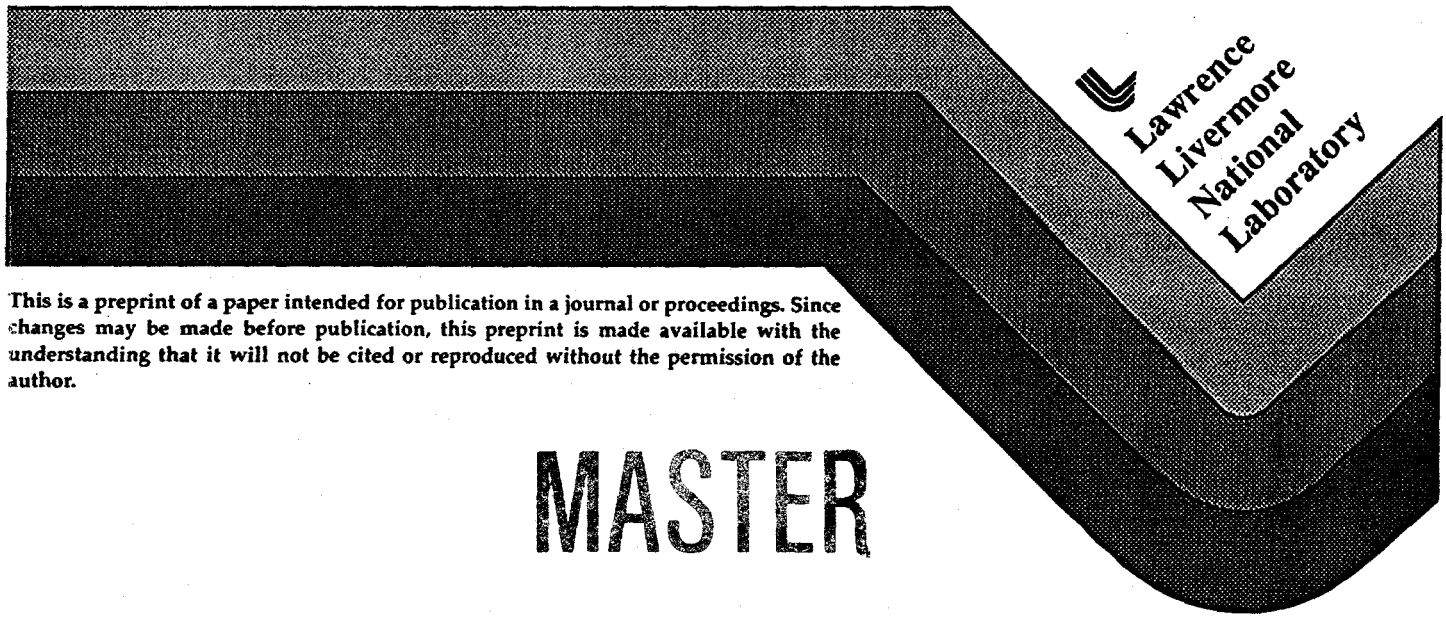

DISCLAIMER

DISCLAIMER

Portions of this document may be illegible in electronic image products. Images are produced from the best available original document.

Hyperspectral Imaging in the Infrared Using LIFTIRS

Charles L. Bennett, Michael R. Carter, David J. Fields

Lawrence Livermore National Laboratory
P.O. Box 808, Livermore, CA. 94551

ABSTRACT

In this article, recent characterization measurements made with LIFTIRS, the Livermore Imaging Fourier Transform InfraRed Spectrometer, are presented. A discussion is also presented of the relative merits of the various alternative designs for imaging spectrometers.

Keywords: Hyperspectral Imagers, Imaging Spectrometers, Imaging FTIR Spectrometers, Infrared Imaging Spectrometers, Hyperspectral Sensors, FTIR Spectroscopy

1. INTRODUCTION

Although a great deal of information about a scene can be deduced from shapes and forms apparent in a two dimensional image, spectral measurements add a useful third dimension. Multispectral imagers, characterized by having only a few spectral channels, such as the sensors on Landsat for example, enable qualitative identification of distinctive terrain features, such as vegetation stress, or mineral species. Hyperspectral imagers, characterized by having a large number of spectral channels, enable definitive identification and quantitative measurement of the composition of objects in the field of view. Infrared hyperspectral imagers are particularly useful for remote chemical analysis, since almost all molecules have characteristic rotation-vibration spectra in the infrared, and a broad portion of the so-called "fingerprint" region of the infrared spectrum lies where the atmosphere is relatively transparent, between 8 and 13 μm, (750 to 1250 cm^{-1}).

Until recently, very few thermal infrared hyperspectral imaging instruments were available. We have recently developed an infrared hyperspectral imager based on an imaging Fourier transform spectrometer, and have begun to perform instrument development tests and field measurements. We have found the technique of imaging FTIR to be quite flexible in terms of the facility for tradeoff of spectral resolution for temporal resolution, with no effect on the degree of spatial resolution. The very high optical throughput characteristic of FT spectrometers in general enables high quality and high speed acquisition of imagery. Indeed, the interferometer need produce little more than an average reduction by 50% (due to the beam splitter) in the intensity of light which reaches the image focal plane.

Another important aspect of the imaging FTIR technique is that all spectral slices of the hyperspectral data cube are manifestly co-registered. This is particularly important to preserve the integrity of spatial/spectral correlation's in the hyperspectral data. An example of the nature of such a hyperspectral data cube is illustrated in figure 1.

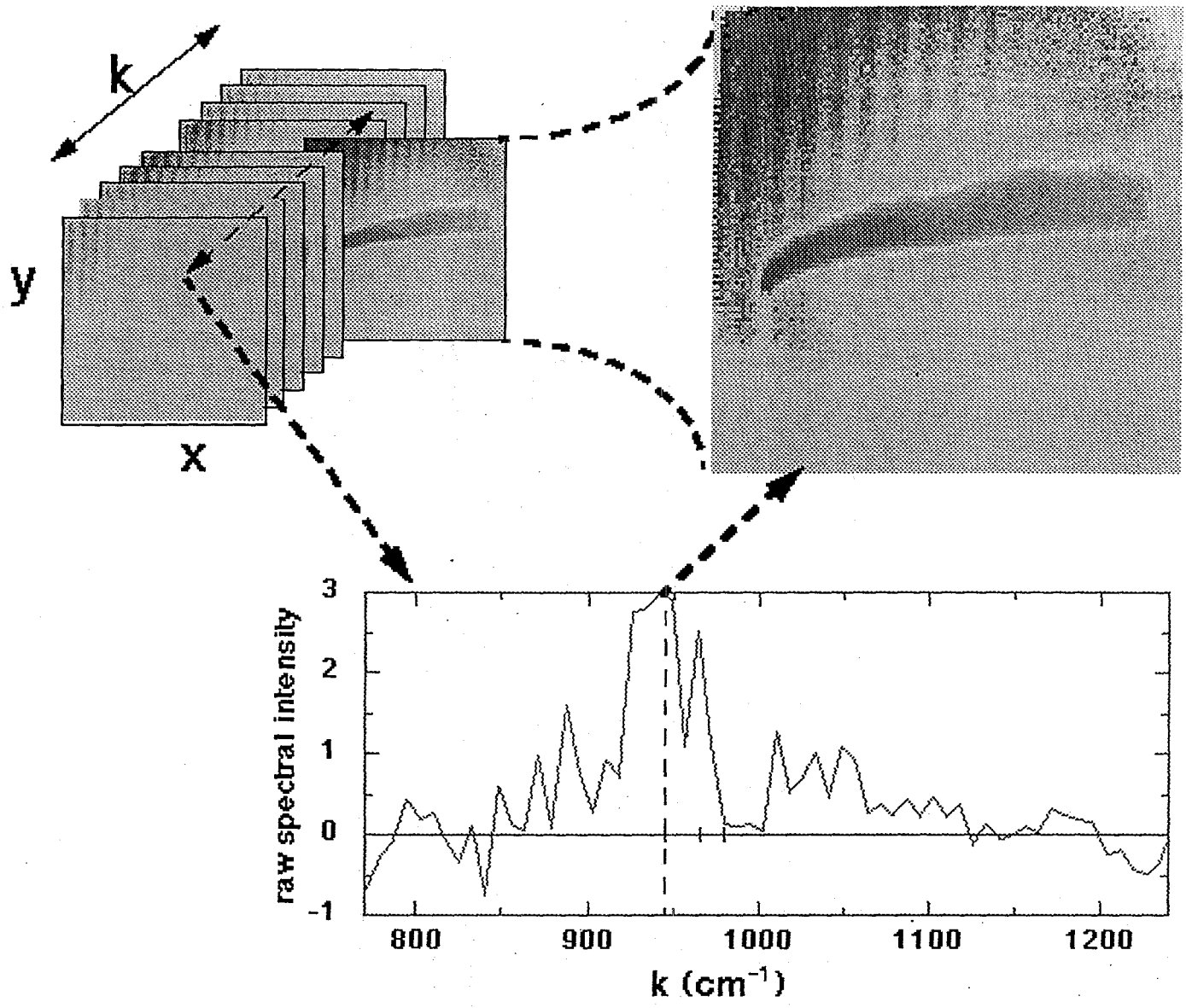

Figure 1. An illustration of hyperspectral imaging. A data cube, as indicated in the upper left of the diagram, consists of a series of images of a scene, each image corresponds to the appearance of the scene as viewed at a given wavenumber k, as is indicated by the arrow extending from the spectral plot to the image in the upper right. On the other hand, a line through the stack of frames in a data cube corresponds to the spectrum of light observed at the corresponding (x,y) location in the image, as is indicated by the arrow piercing the data cube and the downward pointing arrow in the figure.

2. DEVELOPMENT HISTORY

An imaging Fourier transform spectrometer was first described in a 1972 patent by A.E. Potter, Jr[1]. This concept was quite far ahead of its time then, however, and it was not until 1980 that results from a working instrument, with a rather modest 42 element array in the focal plane, were published[2]. Truly "imaging" FTIR spectrometers required the development of relatively large format infrared focal plane array (FPA) detectors. Also, in order to handle the computational demands in a reasonable time, relatively inexpensive, fast computers were needed. As an example, an array of 128x128 pixels generates 16,384 separate interferograms, which must be Fourier transformed to form a spectral data cube. With a single board computer, it is now possible to perform these Fourier transforms as quickly as the data can be acquired.

In 1993, we obtained our first observations with the prototype LIFTIRS instrument. These results, and a general discussion of the advantages and disadvantages of imaging FTIR spectrometers as compared to dispersive hyperspectral imagers were presented at the 1993 SPIE conference in Orlando, Florida[3]. Further results of gaseous effluent imaging and identification were presented at the 1993 SPIE conference in Innsbruck, Austria[4]. The LIFTIRS instrument has been significantly improved since these initial experiments, and detailed discussion of the operational characteristics are discussed by Carter, et al.[5]. The results from some recent field experiments involving gaseous plumes are presented by Bennett, et al[6].

Spaceborne imaging (having at least a few pixels) FTIR spectrometers are discussed by Beer[7], as well as the general theory of FTIR instruments, a comparison with dispersive spectrometers, and a treatment of the general problem of remote sensing through the atmosphere in the infrared portion of the spectrum.

3. GENERIC TRADEOFFS OF IMAGING SPECTROMETER DESIGNS

There are several possible imaging spectrometer designs. These general approaches have basic differences which depend on the manner in which they accumulate the 3 dimensional data cube structure inherent to imaging spectrometers. For ideal instruments making use of 2 dimensional detector FPA's (focal plane array's), a remarkable parity holds for most imaging spectrometer designs. This parity is obtained under the conditions that the only limitation on SNR is pure white quantum statistics noise for each of the possible designs, that all systems enjoy equal total exposure times and entrance aperture sizes, and that the f/# referred to the cone of light converging on the FPA detector elements is the same for all designs. For simplicity, the target spectral radiance is assumed to be constant over a bandpass B, and constant over the imaged area A. For each imaging spectrometer design, the ideal limiting SNR is calculated for a representative cell in the 3 dimensional data cube.

3.1 Temporally modulated imaging Fourier transform spectrometer

Assuming a white noise spectrum, the relation between the signal to noise ratio in the interferogram domain, SNR_x, (defined by the ratio of the maximum swing from baseline in the interferogram at the zero phase difference point for a properly phase compensated interferometer to the rms noise level in the interferogram) and the average in–band signal to noise ratio measured in the spectral domain, SNR_k, is

$$SNR_k\,(TMIFTS) = SNR_x * \frac{\sqrt{N_k}}{m}\ , \qquad (1)$$

where N_k is the total number of spectral channels below the Nyquist limit, which is half the number of interferogram samples N_x, for a two sided interferogram, (it is equal to the number of interferogram samples for a one sided interferogram) and m is the spectral bandpass of the system in units of channels. In the limiting case m=1, only a single spectral component is present. In this case the interferogram is a pure sinusoid. The measurement of N_x points in the interferogram domain improves the signal to noise in the spectral domain by a factor of $\sqrt{N_x}$ over that of a single measurement. The remaining $\sqrt{2} = \sqrt{N_x/N_k}$ factor is obtained since only the real part of the properly phase compensated Fourier transform contains signal, while the noise is evenly divided between real and imaginary components.

3.2 Tunable filter imaging spectrometer

On the other hand, for an ideal tunable filter imaging spectrometer, for which a series of m successive images are acquired through filters of 100% efficiency over their respective non-overlapping pass bands, the total flux on the imager is reduced by the ratio of the filter bandwidth to the total pass band accepted by the imager, given by $\sqrt{m}$. On the other hand, in the same amount of time required for the N_x samples by the Fourier transform instrument, a total of N_x /m sweeps through the bandpass B may be made, leading to

$$SNR_k\,(TFIS) = SNR_x * \frac{\sqrt{N_x}}{m}\ , \qquad (2)$$

where SNR_x is the signal to noise ratio that would be obtained if the complete bandpass B impinged on the imager, and is thus equivalent to the corresponding value in equation (1). An ideal tunable filter imaging spectrometer is thus better by a factor of $\sqrt{2}$ than an ideal Fourier transform imaging spectrometer, which may be attributed to the 50% average transmission of the beam splitter in the Fourier transform spectrometer compared to the 100% ideal filter response for all channels in the tunable filter.

3.3 Dispersive imaging spectrometer

An ideal dispersive spectrometer disperses the bandpass B uniformly across the width of the detector FPA, with no "spillover" or "shortfall". Just as for the tunable filter, the total flux on any given pixel of the FPA is reduced by the ratio of the width of a spectral resolution element to the total bandpass B. Although the dispersive imaging spectrometer acquires all m spectral channels simultaneously, it must scan over N_y spatial lines in order to accumulate an entire data cube. Thus the ideal SNR is given by

$$SNR_k\,(DIS) = SNR_k\,(TFIS) * \sqrt{\frac{m}{N_y}}\ . \qquad (3)$$

For a square format FPA, the radical in equation (3) becomes unity.

3.4 Spatially modulated imaging Fourier transform spectrometer

An ideal spatially modulated Fourier transform spectrometer re-images light emerging from an entrance slit in the object plane in one dimension, and produces an interferogram

along the orthogonal spatial dimension. In order to obtain "square" pixels without anamorphic optics, the aspect ratio of the entrance slit must be no less than N_y, the number of pixels along the slit image. Relative to the intensity that would be obtained by re-imaging the slit on the detector FPA, there is a loss of a factor of N_y in intensity on the average. The number of interferogram points measured is determined by N_x. Thus the ideal SNR becomes

$$SNR_k\,(SMIFTS) = SNR_x * \frac{\sqrt{N_x}}{m\sqrt{N_y}} = SNR_k\,(TFIS) * \sqrt{\frac{1}{m}} \quad (4)$$

3.5 General comparisons and summary

In the limit that all three dimensions of the data cube are equal, $N_x=N_y=m=N_k$, there is little difference in SNR between the first three general designs of imaging spectrometers. The SMIFTS design, however, is intrinsically less efficient. The demands on the detector FPA are substantially different between the four approaches. In the temporally modulated imaging Fourier transform spectrometer, the individual frames are exposed to a much greater signal flux, and thus the noise floor of the FPA is not as critical as for either the dispersive systems or the tunable filter systems. Furthermore, only the first system can be reasonably operated in the thermal infrared portion of the spectrum with ambient temperature optics and detector housings. For applications in the thermal infrared for which there is a premium on cryogenic mass, such as in satellite deployment, this is a great advantage. For the tunable filter system, in contrast to all the other cases, it is possible to "jump around" in wavelength, and thus, in principle, one need only measure the bare minimum of spectral features needed to identify or quantify a given target. The tunable filter, however, is the most sensitive to temporal fluctuations in the target scene, since any time variation appears as a spurious spectral feature. The dispersive imaging systems seem best suited to a "push broom" type of image scanning, wherein the motion of an aircraft or spacecraft is used to provide the cross track sweeping.

The temporally modulated Fourier transform design has the advantage of the greatest flexibility in terms of the choice of spectral resolution. With the current LIFTIRS design it is possible to get imagery with spectral resolution ranging from 0.5 cm^{-1} to 500 cm^{-1} with the same instrument. The adaptability of the spectral resolution is particularly important in cases for which the natural band width of spectral features, their complexity, and distribution across the spectrum is unknown. In general, for a fixed observation time, the SNR per spectral channel varies in direct proportion to the width of the instrumental resolution function. The temporally modulated Fourier transform design also enjoys the brightest imagery of any of the imaging spectrometer designs, since each frame of the interferogram data cube has, on the average, only 50% reduction in intensity compared to an image in the absence of the interferometer. For these reasons, we have particularly concentrated our imaging spectroscopic efforts at Livermore on the LIFTIRS instrument.

Another aspect of the LIFTIRS instrument which we have recently discovered, is that it is possible, from measurements of spectra alone, to correct for differential non-linearity of the individual pixel responses. This is a novel result, and carries implications for the enhanced calibration reliability of temporally modulated Fourier transform instruments in general.

4. NONLINEARITY EFFECTS

One aspect of the current generation of infrared FPA's is the relatively high degree of pixel to pixel non uniformity, as compared, for example, to visible CCD's. The fact that the behavior of the various detector elements in the FPA varies significantly is currently a primary

limitation on the threshold detectability for weak spatial/spectral features in a complex scene. For example, if a simple two point calibration of FPA response is made, a pixel with a substantially differing non-linearity than its neighbors would produce a spurious spectral feature that might show up as a local hot (or cold) spot when viewing a perfectly flat black body at a temperature intermediate between the two calibration points.

One of the features of an imaging FTIR spectrometer such as LIFTIRS is that it is DC coupled to the incident flux rather than AC coupled as in most conventional FTIR spectrometers. The reason for this is that with the large number of pixels in an FPA, it is impractical to have separate detector/amplifier chains for each pixel. Instead, the pixels are multiplexed through a number of channels, e.g. 1,2 or 4, much less than the number of pixels. Because a direct measure of the total flux level on the detector elements may be had from the interferograms, it is possible to perform non-linearity corrections for the response of the individual pixels, since the light level, not just its variations, is known. And, for spectral bandpass widths which are not too large, it is possible from the calculated spectra alone to determine the magnitude and degree of the non-linearity corrections to the detector response.

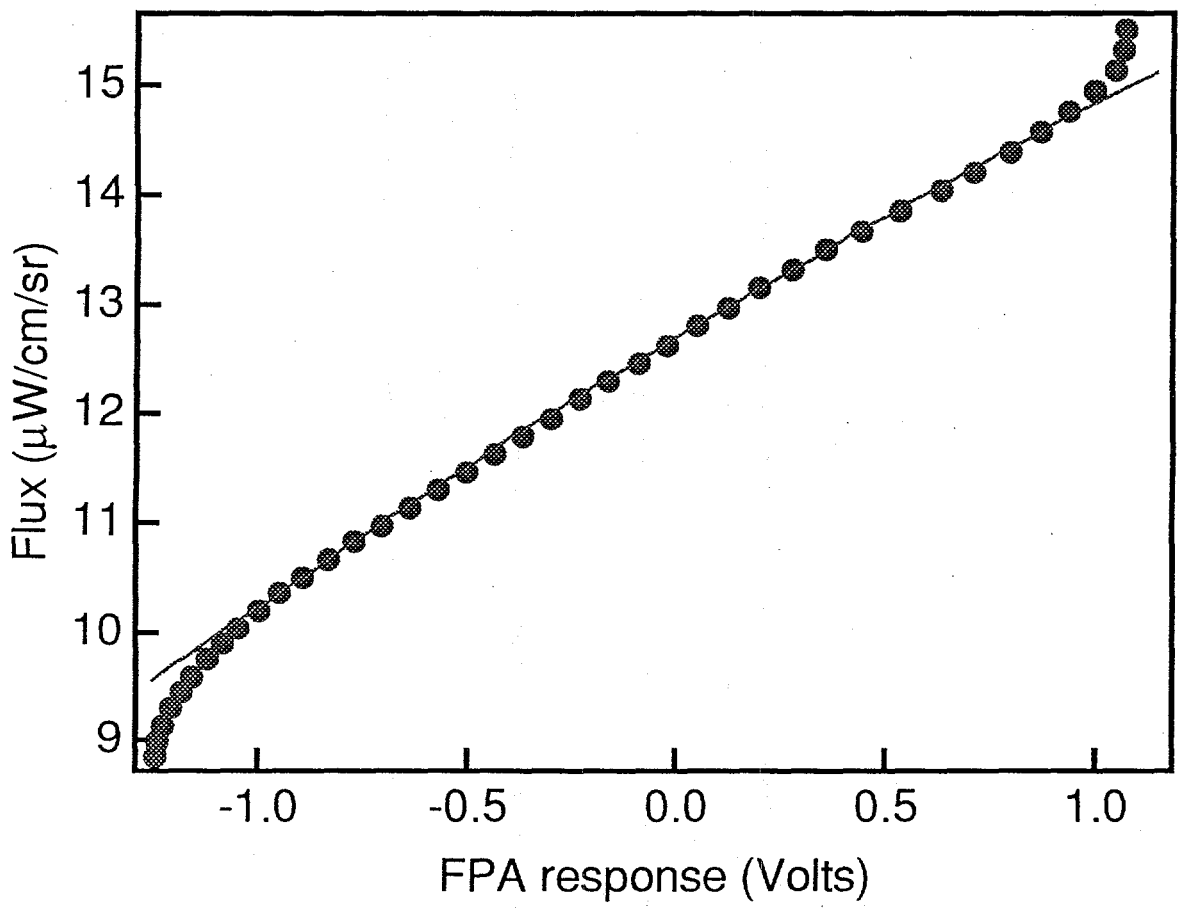

Figure 2. Display of the FPA averaged voltage response (x axis) vs. external blackbody flux level at 9 μm (y axis). For the operating conditions pertaining to this measurement the "working range" extends from 20° C to 42° C.

Figure 2 displays a typical response curve for the Ga:Si FPA which is used in the LIFTIRS spectrometer and which has an 8-13 μm bandpass filter in front of the FPA. In this plot, the measurement error on the individual points is approximately 0.01%. The solid line in this plot represents a quadratic fit to the response over the central "working range". The rms residual error in the quadratic fit to the response over the working range is approximately 0.1%, which corresponds to calibration limited SNR of 1,000 even though the SNR for the individual measurements in this figure is 10,000.

For infrared remote sensing applications, the two main transparent windows in the atmosphere are the 750-1250 cm^{-1} range, and the 2000-3333 cm^{-1} range. Since both of these spectral regions span less than an octave in frequency, it is possible to utilize a unique feature of Fourier transform spectrometers to correct for non-linearity effects on the spectral response. As an example, consider the thermal infrared band from approximately 750 to 1250 cm^{-1}. If a cold bandpass filter is placed in front of the FPA, then the intensity of light impinging on the FPA will contain no frequency components outside the pass band of the filter. Define I(x) as the relative intensity of light incident on the FPA when the optical path difference between the two optical paths in the interferometer differs by a distance x. I(x) may be written in terms of the spectral composition of the light incident on the FPA, S(k), as

$$I(x) = \int_{k_1}^{k_2} S(k)\, \cos(2\pi\, kx)\, dk \quad , \tag{5}$$

where, for simplicity, a constant offset has been suppressed, and all effects of phase dispersion have been ignored. As usual in FTIR spectroscopy, the spectral intensity S(k) can be recovered from discrete samples of the interferogram I(x) by a Fourier transformation. If the measured response, V(I), to the incident intensity is non-linear, however, it is necessary to correct for the non-linearity. For small excursions about a given incident flux, it suffices to consider quadratic corrections only. A quadratic dependence on the incidence flux leads to a contribution of the form

$$I^2(x) = \int_{k_1}^{k_2} \int_{k_1}^{k_2} S(k')\, \cos(\, 2\pi\, k'\, x)\, S(k)\, \cos(\, 2\pi\, k\, x)\, dk\, dk' \quad , \tag{6}$$

which may be rewritten, using the identity,

$$2\, \cos(2\pi\, k\, x)\, \cos(2\pi\, k'\, x) = \cos(2\pi\, (k+k')x) + \cos(2\pi\, (k-k')x), \tag{7}$$

in terms of all possible sums and differences of inband frequencies. For the pass band 750 to 1250 cm^{-1}, the "base band" contribution is restricted to the interval 0 to 500 cm^{-1}, while the "second harmonic band" contribution is restricted to the range 1500 to 2500 cm^{-1}. Similarly, in the presence of a cubic contribution to the non-linearity, a broad "first harmonic" would extend from 250 to 1750 cm^{-1}, and a similarly broad "third harmonic" would extend from 2250 to 3750 cm^{-1}.

As an example of the forms expected for the base band and second harmonic band spectra, in the case that the spectral intensity S(k) is independent of k, both the base band and the second harmonic band are triangular in shape. The second harmonic band would peak at twice the average pass band frequency, while the base band intensity would peak at zero

frequency. This qualitative behavior can be seen in figure 3, which displays the difference between a spectrum calculated with no correction for the non-linearity of the detector, and a spectrum calculated by minimizing the second harmonic spectral power by a one parameter adjustment on the level of the quadratic contribution. It can also be seen in figure 4 that there is very little sign of cubic non linearity, as there would be a "third harmonic" bump peaked at approximately 3000 cm^{-1} in this case. This is consistent with the direct behavior of the FPA response shown in figure 2, which is dominated by the linear and quadratic terms.

As FPA's inevitably have a certain offset response in the absence of external flux, it is necessary to perform at minimum a two point calibration in order to correct for both differential gain and offset variations for all pixels in the array. By using the above algorithm to determine the magnitude of the quadratic response term at both of the calibration points used in a standard two point calibration, it is possible to determine not only the quadratic response term, but also the change in the quadratic term with external flux, which thus provides a measure of the cubic response term. In effect, the functionality of four independent reference calibration sources can be attained with only two reference sources.

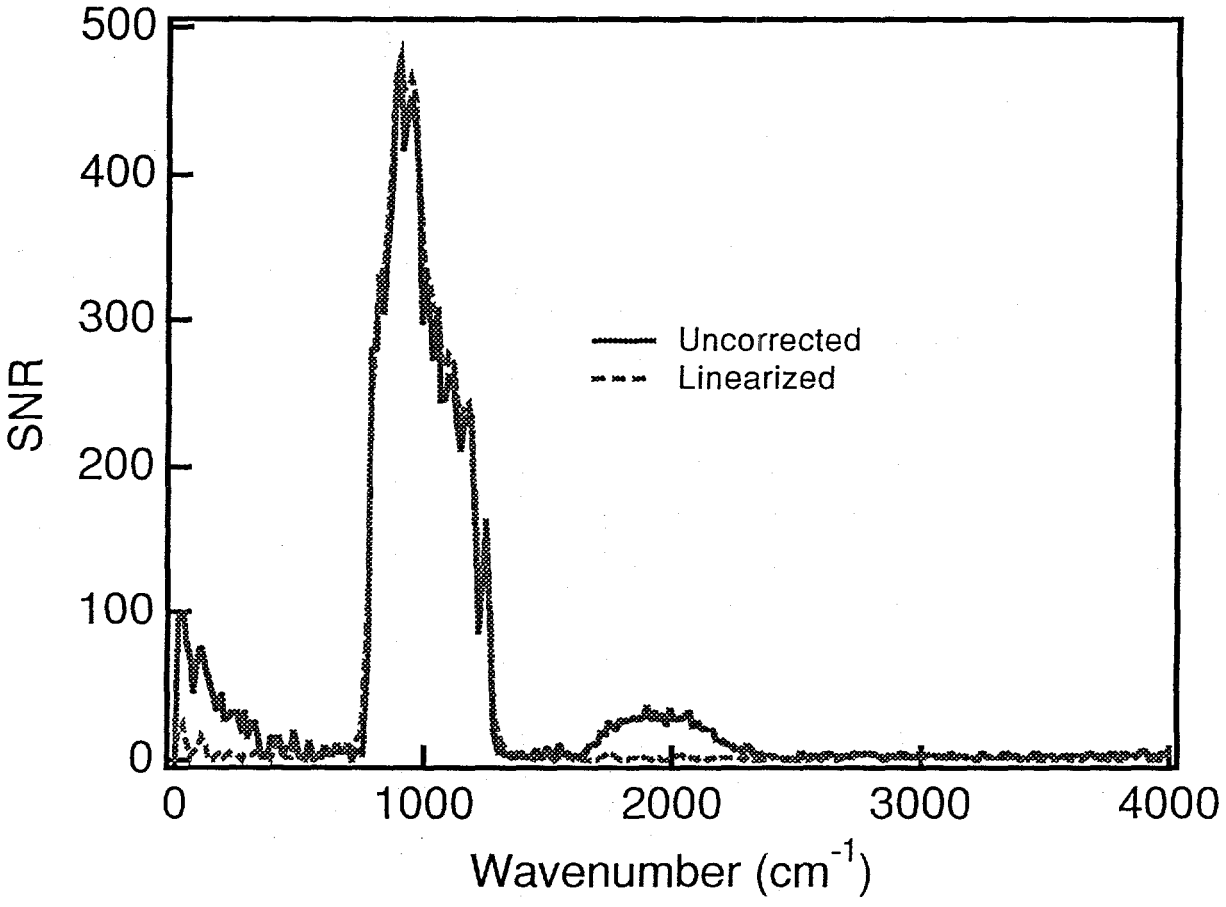

Figure 3. Display of the affect on the spectrum of a single representative pixel after correction for non-linearity effects. The spectral intensity is normalized in units of the rms deviation in the out of band noise level, and represents the signal to noise ratio (SNR) within the 8-13 μm pass band.

5. LIFTIRS CALIBRATION

In a test of the SNR obtainable with LIFTIRS, a series of measurements of a CI Systems black body reference source were made. In one series, the reference black body was set to temperatures of 5° C to 45° C in 5° C increments. All nine measurements consisted of a series of 16 co-added data cubes. The data cubes each consisted of 512 successive frames, with each frame comprising 128x128 spatial pixels. The entire series of data cubes in this test was acquired within a 30 minute time interval. From the 512 point interferograms for each pixel, the signed magnitude of the FFT of the interferogram was used to compute the spectra. For the coldest external black body source it was observed that the signed magnitude spectrum became negative for some spectral and spatial channels. This is consistent with the direction of the energy flow being from the FPA side of the interferometer to the outside world for certain spatial and spectral channels. The residual deviations from flat field behavior over the central 16x16 pixel region in the image, and over the entire range of temperatures from 5° C to 45° C was used to determine the "calibration limited" SNR. The spectral variation of this SNR is displayed in figure 4.

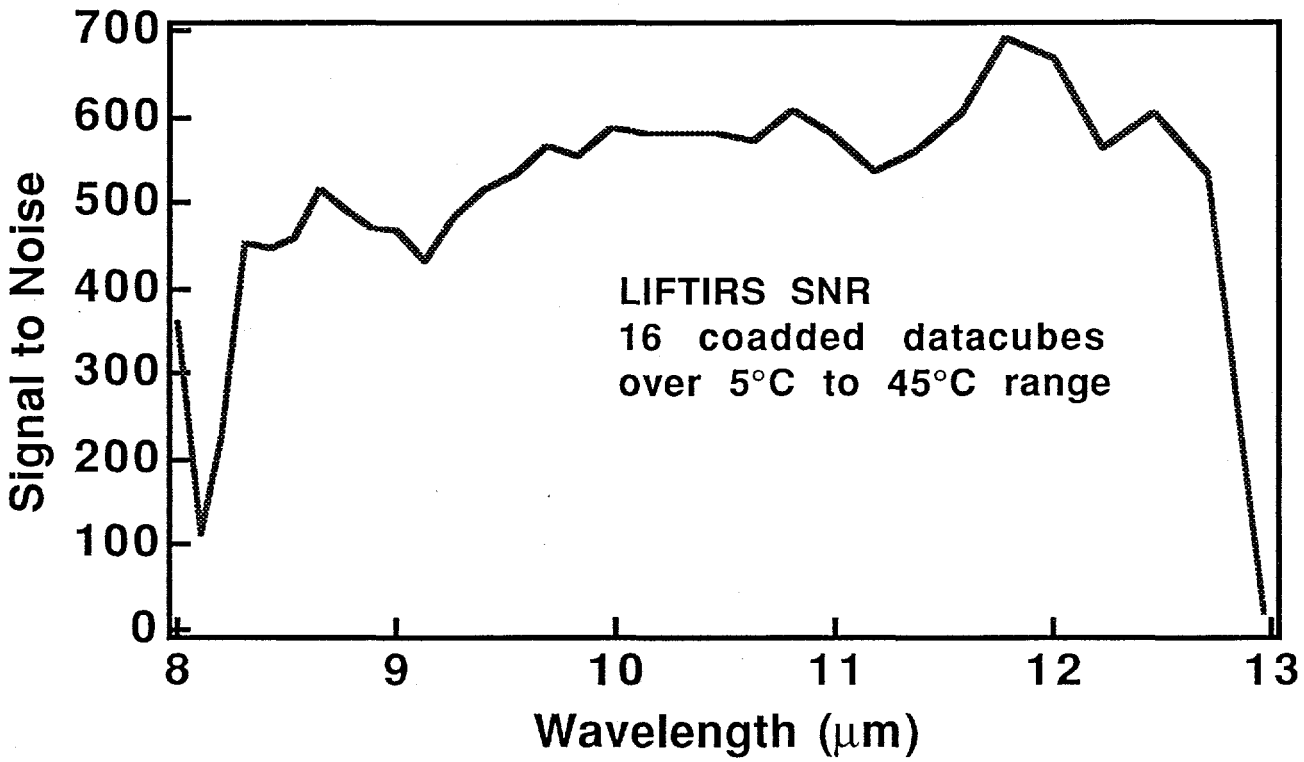

Figure 4. The Signal to Noise ratio obtained with LIFTIRS is plotted as a function of wavelength. This curve represents the average SNR for blackbodies ranging from 5° to 45° C, and is also averaged over a 16x16 subarray of pixels. This data was taken at a resolution of 16 cm^{-1}, with individual scans requiring approximately 1.25 s of acquisition time for a complete 128x128x512 data cube. The notch in the SNR at 8.2 μm coincides with a notch in the transmission of the 8-13 μm band pass filter used to take these measurements.

6. ACKNOWLEDGMENTS

This work was performed under the auspices of the U.S. Department of Energy under Contract No. W-7405-Eng-48. We thank Mark Eckart for providing support for this effort.

7. REFERENCES

1. A.E. Potter, Jr., "Multispectral Imaging System", U.S. Patent # 3702735, Nov. 14, 1972.
2. C.W. Wells, A.E. Potter, T.H. Morgan, "Near-infrared spectral imaging Michelson interferometer for astronomical applications", in the proceedings of the conference: Infrared Imaging Systems Technology, April 10-11, 1980, Washington, D.C., ed. J. Zimmerman, W.L. Wolfe, SPIE vol 226.
3. C.L. Bennett, M. Carter, D. Fields, J. Hernandez, "Imaging Fourier Transform Spectrometer", p.191-200, in the proceedings of the Imaging Spectrometry of the Terrestrial Environment, April 14-15, 1993, Orlando, Fl., SPIE vol 1937.
4. M.R. Carter, C.L. Bennett, D.J. Fields, J. Hernandez, "Gaseous effluent monitoring and identification using an imaging Fourier transform spectrometer", p.16-26, in the proceedings of the Substance Detection Systems, October 5-8, 1993, Innsbruck, Austria, SPIE vol 2092.
5. M.R. Carter, C.L. Bennett, D.J. Fields, D. Lee, "Livermore Imaging Fourier Transform Infrared Spectrometer (LIFTIRS)", in the proceedings of Imaging Spectrometry, April 17-19, 1995, Orlando, Fl., SPIE vol 2480, pp. 380-386.
6. C.L. Bennett, M.R. Carter, D.J. Fields and F.D. Lee, "Infrared hyperspectral imaging results from vapor plume experiments", in the proceedings of Imaging Spectrometry, April 17-19, 1995, Orlando, Fl., SPIE vol 2480, pp. 435-444.
7. Reinhard Beer, Remote Sensing by Fourier Transform Spectrometry, John Wiley & Sons, Inc., NY, 1992.